Plasmonic Near-Field Absorbers for Ultrathin Solar Cells

ARTICLE *in* JOURNAL OF PHYSICAL CHEMISTRY LETTERS · MAY 2012

Impact Factor: 7.46 · DOI: 10.1021/jz300290d

2 AUTHORS:

Carl Hägglund
Uppsala University
37 PUBLICATIONS **923** CITATIONS
SEE PROFILE

Peter Apell
Chalmers University of Technology
204 PUBLICATIONS **3,472** CITATIONS
SEE PROFILE

THE JOURNAL OF PHYSICAL CHEMISTRY Letters

Perspective

pubs.acs.org/JPCL

Plasmonic Near-Field Absorbers for Ultrathin Solar Cells

Carl Hägglund*,† and S. Peter Apell‡

†Department of Chemical Engineering, Stanford University, Stanford, California, 94305, United States

‡Department of Applied Physics, Chalmers University of Technology, SE-412 96 Göteborg, Sweden

Supporting Information

ABSTRACT: If the active layer of efficient solar cells could be made 100 times thinner than in today's thin film devices, their economic competitiveness would greatly benefit. However, conventional solar cell materials do not have the optical capability to allow for such thickness reductions without a substantial loss of light absorption. To address this challenge, the use of plasmon resonances in metal nanostructures to trap light and create charge carriers in a nearby semiconductor material is an interesting opportunity. In this Perspective, recent progress with regards to ultrathin (~10 nm) plasmonic nanocomposites is reviewed. Their optimal internal geometry for plasmon near-field induced absorption is discussed, and a zero thickness effective medium representation is used to optimize stacks including an Al back reflector for photovoltaics. This shows that high conversion efficiencies (>20%) are possible even when taking surface scattering effects and thin passivating layers inserted between the metal and semiconductor into account.

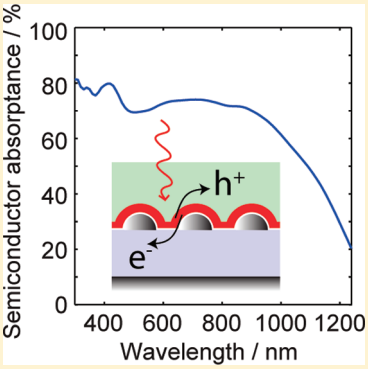

Photovoltaic solar cells have great potential to contribute to a long-term sustainable energy system.[1] However, for a timely impact on a global scale, certain critical challenges reaching beyond a high energy conversion efficiency must be successfully coped with. Factors such as raw material abundance, production costs, and solar cell lifespan all importantly contribute to the (levelized) cost of solar electricity and thus play decisive roles in the large-scale applicability and viability of photovoltaic technology. It is therefore vital to explore concepts allowing for a high conversion efficiency to be realized in economical and resource efficient ways by minimization of the cost and amount of material used. In this respect, the use of localized surface plasmon resonances is of high current interest.[2]

In any solar energy conversion device, light absorption is the first of a sequence of events leading to useful energy output in the form of fuel, electricity, or heat. The ability to absorb light is what typically dictates the minimum amount of material needed to form the photoactive layer of the device. This material requirement is fundamentally connected to a minimum requirement of the number of electrons (oscillator strength[3]) contributing to the absorption cross section over the spectral range of importance for solar energy conversion. From arguments along these lines, and, more precisely, the Thomas-Reiche-Kuhn sum rule,[3] the smallest amount of absorber material needed for complete absorption has been estimated as that contained in a film of characteristic thickness around 10 nm.[4] This is a factor of 100 less than typically used in today's state-of-the-art thin film solar cells.

Part of this thickness mismatch can be ascribed to a "waste" of oscillator strength in conventional solar cell materials spent on optical transitions in spectral regions of little benefit for the conversion of sunlight. From this viewpoint, the localized surface plasmon resonances occurring in the confined volume of metal nanoparticles are of particular interest. They coherently engage the metal conduction electrons as a collective, and especially for the coinage metals Au, Ag, and Cu, a large fraction of the conduction electron oscillator strength can readily be tuned into the proper spectral range by adjustment of particle size, shape, and local environment. Because such a large number of electrons are involved in these resonances, the optical cross sections for absorption and scattering can be large, even exceeding the projected geometrical area of a plasmonic particle over an appreciable spectral range. Thus a key opportunity of plasmon resonances lies in their ability to condense the conduction electron oscillator strength into the desired spectral range for photovoltaics, in principle making it possible to approach the "10 nm limit" for efficient solar cells. Apart from resource and processing savings, the benefits of such a prospect include the possibility to use new and cheaper materials with shorter carrier mean free paths and also potentially higher open circuit voltages due to the concentrated absorption.[5]

A key opportunity of plasmon resonances lies in their ability to condense the conduction electron oscillator strength into the desired spectral range for photovoltaics, in principle making it possible to approach the "10 nm limit" for efficient solar cells.

Received: March 12, 2012
Accepted: April 26, 2012

   dx.doi.org/10.1021/jz300290d | J. Phys. Chem. Lett. 2012, 3, 1275–1285

Much of the essential physics of localized plasmons can be understood in terms of a classical electromagnetic response of the conduction electron cloud. It is in the small particle/long wavelength limit oscillating in a dipolar mode.[6] Apart from light absorption and scattering, the induced surface charge distributions create dramatically enhanced electric field strength just outside the particle, as illustrated in a calculation by the finite element method (FEM) in Figure 1a. An important

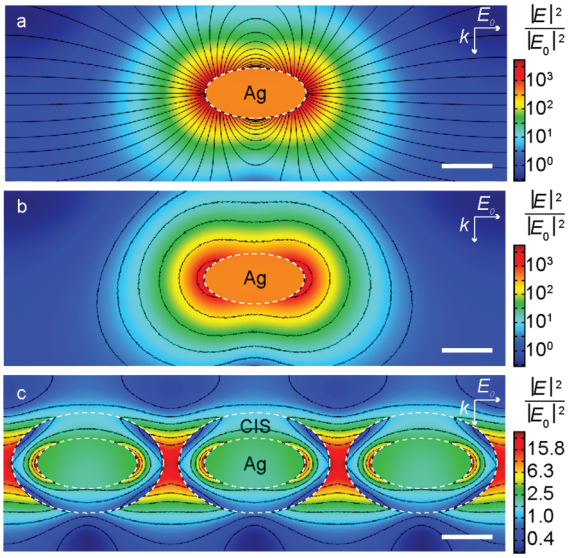

Figure 1. For solar cell applications, the electric field energy distribution is important for the transfer of incident photons to electronic excitations. The electric field energy distributions calculated by the FEM are here shown for cross sections of small Ag spheroids (40 nm diameter and 20 nm height, dashed white outline) excited in a mainly dipolar mode by an incident plane wave field E_0 propagating with wave vector k. The black field line pattern exhibited in panel a is characteristic of a dipole resonance. In panel b, the black, shell-like contours represent isosurfaces of constant electric field energy for the same system. In panel c, the corresponding field energy map and isosurfaces are shown in the cross section of a planar, square array of core/shell particles of a typical plasmonic metal (Ag) and thin film solar cell semiconductor ($CuInSe_2$ or CIS for short, with inner and outer boundaries marked by dashed white lines). The CIS shell thickness is 10 nm. Scale bars are 20 nm, and the wavelengths were chosen close to the plasmon resonances, at 426 nm in panels a and b and 676 nm in c.

question for photovoltaic applications is to what extent these effects can be exploited for charge carrier generation, that is, how well the oscillator strength condensed into plasmon resonances lends itself to the creation of single electron−hole pairs (excitons) useful in a solar cell.

The creation of useful charge carriers by means of plasmons typically involve a sequence as follows: incident photon → excitation of plasmon → creation of exciton → separation of charge carriers. This can be realized using one of three approaches based on where the excitons are created, namely, (1) internally in the metal nanostructure, (2) externally in the electromagnetic near-field region,[7] and (3) further away in the far-field region.[7] In approach 1, the internal plasmon decay to a single electron−hole pair inside the metal is used to create an emission of either a hot electron or hole across the metal surface. In this way, significant charge carrier separation has been suggested to occur.[8,9] This is in competition with the otherwise rapid electron−hole pair cascade leading to the formation of heat in the metal.[10,11] The near-field route 2 instead exploits the generation of electron−hole pairs in a semiconductor material located in close proximity to the metal, and has recently been investigated for some different configurations.[12−18] A strong coupling mediated by the near-field allows for efficient "exchange" of oscillator strength such that Joule heating of the metal can be reduced in favor of more long-lived electron−hole pairs being excited in the semiconductor.[4] The proximity of the semiconductor to the metal surface may, due to surface recombination, on the other hand, reduce the lifetime of these electron−hole pairs significantly as compared to the lifetimes in bulk semiconductors, unless passivation is accomplished. The far-field route 3 avoids the latter issue by separating the metal and semiconductor. In this case, the scattering induced by the plasmon resonances can be exploited to trap light in guided propagating modes with an optical path length through the solar cell absorber layer that is effectively enhanced. Approaches along the latter lines, initiated by Stuart and Hall,[19] have been covered in more depth elsewhere.[2,20,21]

The present Perspective focuses on recent work in the area of plasmonic near-field absorbers for solar cells. Beginning with a discussion of the optimal internal geometry of ultrathin metal/semiconductor nanocomposite films when aiming to minimize the amount of absorber material required, the paper continues by addressing some general aspects of light absorption in such films, how the absorption rates distribute locally within nanocomposites, and the broadband optimization of these systems toward photovoltaic applications. Special attention is directed to the effects of surface scattering and inclusion of optically inert barrier layers in the design. An outlook toward important challenges and future opportunities for solar cells concludes the paper.

With the objective to minimize the amount of material in a solar cell absorber layer by use of plasmonic nanoparticles, a critical aspect is to optimize the geometry such that the average absorption rate in the semiconductor volume is maximized. This implies that it is desirable to distribute the semiconductor material such that it is, in the end, bounded by an isosurface of constant local absorption rate. If absorbing material would be moved outside such a boundary, its absorption rate, and thereby the overall average, would decrease.[15] In a nonmagnetic material, the absorption rate is proportional to the electric field energy density ($\sim|E|^2$, with E being the electric field amplitude).[7] Figure 1b shows calculated isosurfaces defining constant electric field energy, which are seen to enclose regions of most intense field energy near the particle poles as defined by the polarization direction of the incident field. Slightly further out, these isosurfaces expand to enclose the entire particle, defining shells of increasingly uniform thickness. The dipolar field distribution is a general feature in the small particle limit, although for metal particles, the polarizability and thus scattering and absorption vary strongly with particle shape, orientation, and the wavelength of light.[6] However, the total integrated field energy inside the metal particle compared to the corresponding measure for the surrounding medium is not dependent on metal particle shape as long as a particular plasmon resonance frequency is considered.[22] Because of this, round metal particle shapes such as spheroids can be expected to be as good as more pointy nanostructures for inducing absorption in nearby semiconductor material, given that the

dx.doi.org/10.1021/jz300290d | J. Phys. Chem. Lett. 2012, 3, 1275−1285

semiconductor can be considered a "surrounding medium" to some approximation. When adding a semiconductor shell or arranging the particles into an array, the simple shell-like isosurfaces are deformed, but do still provide a decent description of the absorption distribution close to the metal particles (Figure 1c). Hence shells of uniform thickness surrounding spheroidal metal cores come close to the ideal for maximizing the plasmon near-field induced absorption rate in the semiconductor, especially when taking into account that the degree of polarization is low for sunlight and that the angle of incidence varies in actual applications. Another practical advantage of this is that high-quality uniform coatings of many semiconductor materials are quite feasible to accomplish, for instance by atomic layer deposition.[23] Finally, from a theoretical standpoint, core/shell nanoparticle arrays are relatively straightforward to analyze. For these reasons, this system (Figure 2a,b) is a

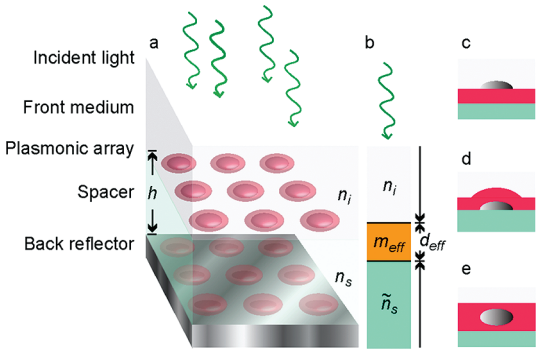

Figure 2. (a) Array of metal core/semiconductor shell nanoparticles representing a close to ideal plasmonic near-field absorber. The absorber is supported by a spacer (typical thickness h ~100 nm, refractive index n_s) on a highly reflective support. (b) An ultrathin (~10 nm) plasmonic absorber may be represented as an effective medium of complex refractive index m_{eff} and near-zero effective thickness d_{eff}. The combined properties of the spacer and reflector can also be captured by an effective refractive index $\tilde{n}_s$. Alternative unit cells for the absorber (semiconductor colored red) include (c) a plasmonic particle on top of a planar semiconductor layer, (d) a semiconductor coated plasmonic particle, and (e) a plasmonic particle embedded in the semiconductor layer.

model system of high interest. However, as discussed further below, it turns out that the details of the absorber layer geometry are not that critical in the long wavelength limit,[15] and alternative configurations more common in experimental works[17,24,25] (Figure 2c–e) may be of higher interest in the end.

Round metal particle shapes such as spheroids can be expected to be as good as more pointy nanostructures for inducing absorption in nearby semiconductor material, given that the semiconductor can be considered a "surrounding medium" to some approximation.

To further analyze the type of core/shell nanoparticle arrays illustrated in Figure 2a, one may exploit that small particles (that is, much smaller than the wavelength λ of light) arranged in a planar array with a relatively small lattice constant (smaller than the wavelength in the surrounding media), may, to good approximation, be represented as a very thin, homogeneous layer having a complex refractive index $m_{eff} = n_{eff} + i\kappa_{eff}$ and an effective thickness d_{eff} (Figure 2b).[26] The electrostatic point dipole approximation for the particle polarizabilities[6] and the analysis of interacting dipoles in a square array provided by Vlieger[27] allows a simple expression for the effective medium properties of the array to be derived.[4,28] In brief, the effective refractive index of the array at normal incidence of light is given by

$$n_{eff} + i\kappa_{eff} \approx n_e\left(\frac{3\alpha}{(3\Lambda^3/4\pi - G\alpha)}\frac{\Lambda}{d_{eff}}\right)^{1/2} \quad (1)$$

where $G = 1.08$ for a square array with array constant Λ.

The factor G varies only slightly with the array type, making eq 1 approximately correct for arbitrary lattices of dipole-like particles, provided Λ is obtained from the particle surface density ρ through $\Lambda = \rho^{-1/2}$ and that $\Lambda < \lambda/n_e$. A common refractive index n_e is here assumed for the surrounding media, but this may be generalized to nonequal refractive indexes surrounding the array by use of an effective value for n_e as devised by, for instance, Vernon et al.[29] The particle polarizability α contains the wavelength dependence, and may describe any type of small nonmagnetic particles in the electrostatic limit.[6] For its determination in the special case of core/shell nanoparticles, the approximation by a confocal system is useful.[30,31]

Equation 1 does not determine the effective properties uniquely unless the effective thickness d_{eff} is set by some additional constraint or measurement. Numerically, if the particles are considered point dipoles, the consistent choice is to evaluate physical expressions (absorptance, reflectance etc.) in the limit as d_{eff} approaches zero.[4] For comparison of these approximations with experiments, measured values of n_{eff}, κ_{eff}, and d_{eff} can also be obtained using techniques such as spectroscopic ellipsometry.[32]

Having described the plasmonic array in terms of an ultrathin film with an effective refractive index given by eq 1, its interaction with normal incident light can be analyzed in terms of reflectance, transmittance, and absorptance in a planar geometry. In the general situation where a planar film is surrounded by two different dielectrics with refractive indexes n_i (in front) and n_s (behind), respectively, the condition for maximizing the absorption of normal incident light was shown to be given by[4]

$$n_{eff} + i\kappa_{eff} \approx \frac{(1+i)(n_i+n_s)^{1/2}}{\sqrt{2}}\left(\frac{\lambda_0}{2\pi d_{eff}}\right)^{1/2} + \frac{(1-i)(n_i^3+n_s^3)}{6\sqrt{2}(n_i+n_s)^{3/2}}\left(\frac{2\pi d_{eff}}{\lambda_0}\right)^{1/2} \quad (2)$$

where λ_0 is the vacuum wavelength. For small effective film thicknesses $d_{eff} \ll \lambda_0$, the first term dominates and represents an optimum that is symmetric about $n_{eff} \approx \kappa_{eff}$, as illustrated in Figure 3a. The optimum corresponds to a strongly damping film material with an almost purely imaginary permittivity $\varepsilon_{eff} = n_{eff}^2 - \kappa_{eff}^2 + 2in_{eff}\kappa_{eff} \approx 2in_{eff}\kappa_{eff}$ reminiscent of epsilon

dx.doi.org/10.1021/jz300290d | J. Phys. Chem. Lett. 2012, 3, 1275–1285

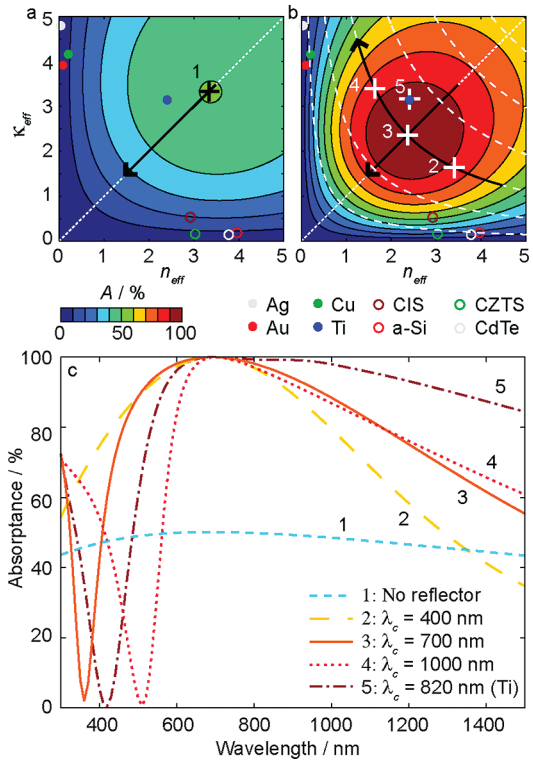

Figure 3. (a) Absorptance at a wavelength of 700 nm versus effective optical constants of a thin film (d_{eff} = 10 nm) in vacuum ($n_i = n_s = 1$, no reflector). The absorptance peaks slightly above 50% at "1", and is symmetric about $n_{eff} = \kappa_{eff}$ (dotted white line). For thicker films, the peak shifts to less damping materials (black arrow). The optical constants of a few materials are indicated for reference (see further Figure 4). (b) Absorptance after adding a spacer (n_s = 1) and ideal reflector behind the film. The spacer thickness is such that the center wavelength λ_c = 700 nm, again producing a symmetric absorptance about $n_{eff} = \kappa_{eff}$, but now with a maximum of 100% at "3" from eq 5. For increasing spacer thickness, the optimum traces a constant optimal damping $2n_{eff}\kappa_{eff}$ (curved dashed lines), toward higher κ_{eff} (curved arrow); with λ_c = 400 nm, the optimum occurs at "2" and with λ_c = 1000 nm it occurs at "4". The spectra in panel c show the thin film absorptance as a function of wavelength for optical constants given by the optima marked in panels a and b. n_{eff} and κ_{eff} were assumed independent of wavelength, except for the Ti film having assumed bulk Ti properties. A Ti thickness of 7.3 nm and λ_c = 820 nm produce critical coupling at λ_0 = 700 nm ("5" in b).

near-zero metamaterials.[33] It results in an absorptance only weakly dependent on d_{eff} according to[4]

$$A_{max} \approx \frac{n_i}{n_i + n_s}\left[1 + \frac{n_s}{6}(3n_s - n_i)\left(\frac{2\pi d_{eff}}{\lambda_0}\right)^2\right] \quad (3)$$

Interestingly, this implies that the maximum achievable absorption is, to a good approximation, determined by the contrast of the refractive indexes for the external media surrounding the film, at least as long the film thickness is less than a few percent of the vacuum wavelength. In practice, however, the achievement of a strong refractive index contrast of the surrounding media is not always feasible, in which case eq 3 shows that the maximum absorptance will end up in the neighborhood of 50%.

To accomplish closer to 100% absorption, one possibility is to add a reflecting layer a distance h (similar to a quarter of a wavelength) behind the ultrathin absorber, such that an optical cavity is created (Figure 2a). This configuration represents an optical analogue to the (electric) Salisbury screen well-known from radar and microwave technology.[34,35] The effect of the dielectric spacer (refractive index n_s) with an assumed ideal back reflector is, at normal incidence, equivalent to an optically thick medium having an effective refractive index[28]

$$\tilde{n}_s(\lambda) = in_s \cot\left(\frac{\pi\lambda_c}{2\lambda}\right) \quad (4)$$

where $\lambda_c = 4n_s h$ defines the wavelength λ_c at which the quarter wave condition is fulfilled for the spacer. The center wavelength λ_c corresponds to the center energy E_c of the fundamental band defined by the pole at $\lambda = \lambda_c/2$ and $\lambda = \infty$ (that is, a band of width $2E_c$). Because $\tilde{n}_s(\lambda)$ is purely imaginary, incident light has only evanescent, nonpropagating field components in the direction into the cavity. This is consistent with the transmission being blocked by the reflector and holds true regardless of wavelength within the band, so the optical path length in the effective medium described by eq 4 is zero and wavelength independent. For this reason, when adding to the cavity an ultrathin absorbing film that also has a near zero optical path length,[4] there is no optical round-trip, Fabry–Perot-type interference condition setting the limit to the absorption bandwidth, which is rather ultimately equal to the cavity bandwidth $2E_c$. The insensitivity to optical path length also translates to a generous angular response.[28] With this support for the absorbing film, the condition for maximum (100%) absorption at λ_0 differs only nominally from the optimum without a reflector. It is given by[28,35]

$$n_{eff} + i\kappa_{eff} \approx \frac{1 + i}{\sqrt{2}}\left(\frac{n_i - \tilde{n}_s}{2\pi d_{eff}}\lambda_0\right)^{1/2} \quad (5)$$

or, in terms of the relative permittivity, $\varepsilon_{eff} = i\lambda_0(n_i - \tilde{n}_s)/(2\pi d_{eff})$. The perfect absorption condition represented by eq 5 is sometimes referred to as critical coupling.[36,37] The absorptance, obtained as $A = 1 - |\tilde{r}|^2$, where $\tilde{r}$ is the reflection coefficient for the absorber, spacer and reflector layers as a whole (taking internal multiple reflections in all layers into account), is shown in Figure 3b as a function of the absorber layer n_{eff} and κ_{eff}. It displays a broad symmetric maximum again peaking for an almost purely damping film permittivity ($n_{eff} \approx \kappa_{eff}$) when $\lambda_c = \lambda_0$. This corresponds to the classical Salisbury screen realization with a quarter wave spacer.

However, the addition of a reflector not only provides an opportunity to absorb nearly 100% of the incident light at λ_0, but the choice of λ_c can also be used to tweak the shape of the absorption spectrum. Because the absorptance has a minimum at $\lambda_c/2$ and a maximum at λ_0, a thicker spacer such that $\lambda_c > \lambda_0$ pushes the absorption peak weight toward the red side of the spectrum. Conversely, the peak skews toward the blue with $\lambda_c < \lambda_0$. This is exemplified in Figure 3c.

On the other hand, in the common situation that the only property of the absorber layer that can be modified is its (effective) thickness, the center wavelength λ_c may provide the additional parameter needed to match the critical coupling condition to the absorber material at hand. To this end, the film thickness d_{eff} is exploited to achieve optimal damping at λ_0 through $\mathrm{Im}(\varepsilon_{eff}) = 2n_{eff}\kappa_{eff} = n_i\lambda_0/(2\pi d_{eff})$, while λ_c is chosen to match the optimum for the real part of the film permittivity $\mathrm{Re}(\varepsilon_{eff}) = n_{eff}^2 - \kappa_{eff}^2 = n_s\lambda_0/(2\pi d_{eff}) \times \cot(\pi\lambda_c/2/\lambda)$ along an orthogonal trajectory of constant damping. This is all illustrated in Figure 3b. In this way, critical coupling is possible to achieve

with homogeneous and ultrathin films of many lossy metals. An example is the 7.3 nm thick Ti film exhibited in Figure 3b,c (that is, to the extent that a uniform thickness and bulk optical constants are appropriate). Apart from lossy metals, some more exotic conductors (such as NbN[38]) exhibit sufficient damping in the visible/near-infrared range to allow for nearly perfect absorption in homogeneous ultrathin films. When it comes to semiconductors, the examples are more scarce. But, a bandgap material in the form of a 5-nm-thick J-aggregated layer of dye has also been demonstrated in which a high oscillator strength condenses into a very narrow line width transition providing the conditions to fulfill eq 5 for a wavelength in the visible.[36]

In contrast to lossy metals, typical thin film solar cell semiconductors such as those exhibited in Figure 3 would unfortunately require much (~10 times) thicker layers to match the critical coupling condition of eq 5, in which case the underlying assumption of an ultrathin absorber film is further not applicable. Even thicker films would be needed with a dielectric medium ($n_i > 1$) in front of the absorber. Thus, to achieve critical coupling in ultrathin layers comprising semiconductors, one is generally forced to consider heterogeneous systems. Noting that the plasmonic metals ($n \ll \kappa$) maps almost diametrically about the symmetry line compared to thin film solar cell semiconductors ($n \gg \kappa$) in Figure 3a,b, it is not too surprising that nanocomposites combining a plasmonic metal with a semiconductor (or for that matter a dielectric or just air) may effectively produce the right conditions ($n_{eff} \approx \kappa_{eff}$). Indeed, by use of ultrathin plasmonic nanostructures, the optimal conditions of both eqs 2 and 5 can be matched. For the case of the spheroidal core/shell nanoparticle arrays described by eq 1, the array can be tuned to generate (in the limit $d_{eff} \to 0$) the optimal conditions by choice of the plasmonic absorber geometry, that is, by selecting metal particle size, eccentricity, the ratio of semiconductor to metal volume, and array density.[4,28] Related configurations shown to accomplish this have included metal nanoparticle arrays on ultrathin planar semiconductor layers (Figure 2c),[15] ordered metal strip,[39] metal nanoparticle arrays in dielectric media,[40,41] and disordered metal/dielectric nanocomposites.[37,42]

Recently, nearly perfect absorbers by means of metal/dielectric metamaterials have also gained attention.[43−46] In these cases, broadband absorptance with a wide angular response in geometries qualitatively similar to the Salisbury screen configuration of Figure 2a has been demonstrated. However, these observations have been attributed to a magnetic metamaterial response (the role of which is still under some debate[47]) rather than the electric-type resonance realized by an optimization according to eq 5. Thinner spacer layers are typically used in these magnetic resonance characterized systems, with a resonance field distribution more centered in the spacer gap than on the plasmonic array. The consequence is more evenly distributed absorption over the array and reflector layers.[48] The metal structures involved are usually also significantly higher than 10 nm, supporting higher order resonances[49] that are not possible in the ultrathin absorber/perfect reflector situation accounted for by eq 5.

Summarizing the above, it is feasible to critically couple ultrathin (~10 nm) metallic film and metal/semiconductor nanocomposites to incident light and produce nearly perfect absorption in the film by means of a back reflector. The implications for solar cells depend on the possible processes following light absorption. If photoemission of hot charge carriers generated by absorption or plasmon decay in ultrathin metal nanostructures can be made efficient enough, purely metallic nanostructures could alone provide the absorption required for efficient solar cells to be realized. As the inelastic mean free paths for hot charge carriers readily exceeds 10 nm in metals at optical energies,[50] this possibility warrants further investigation with the main challenges relating to charge separation.[51] The near-field approach may provide better chances for a high quantum efficiency since the lifetimes of electron−hole pairs generated directly in a semiconductor layer are much longer than in a metal. A critical question is then, how high of a fraction of the aggregated absorption can be channeled to the semiconductor part of the metal/semiconductor nanocomposite?

To address this branching ratio, the fraction of light absorbed in an individual constituent of an ultrathin nanocomposite can be numerically estimated based on the fact that the local absorption rate in nonmagnetic materials is proportional to the damping part of the permittivity, $\mathrm{Im}(\varepsilon)$.[4,28] For a given metal/semiconductor nanocomposite geometry fulfilling the critical coupling condition, a case is considered where the metal damping $\mathrm{Im}(\varepsilon_{met})$ is artificially set to zero. The semiconductor damping $\mathrm{Im}(\varepsilon_{sc})$ is then artificially increased to the value $\mathrm{Im}(\varepsilon_{sc}{}^0)$, which is required to reestablish the critical coupling condition of eq 5. This should be done without altering the plasmon peak wavelength, which is approximately accomplished if leaving the semiconductor refractive index (n_{sc}) fixed in the process. The difference $\mathrm{Im}(\varepsilon_{met}{}^*) \equiv \mathrm{Im}(\varepsilon_{sc}{}^0) - \mathrm{Im}(\varepsilon_{sc})$ represents the damping of the metal core had this damping instead been distributed in the space of the semiconductor. The determination of $\mathrm{Im}(\varepsilon_{met}{}^*)$ in this way allows for a direct comparison with the actual semiconductor damping $\mathrm{Im}(\varepsilon_{sc})$. The branching ratio for semiconductor absorption at the peak is thus simply obtained from $\mathrm{Im}(\varepsilon_{sc})/[\mathrm{Im}(\varepsilon_{met}{}^*) + \mathrm{Im}(\varepsilon_{sc})] = \mathrm{Im}(\varepsilon_{sc})/\mathrm{Im}(\varepsilon_{sc}{}^0)$. It is clear that if a high branching ratio is desired, the metal damping should be as small and the semiconductor damping as high as possible. The bulk damping as a function of wavelength is given in Figure 4 for common plasmonic metals and thin film solar cell materials.

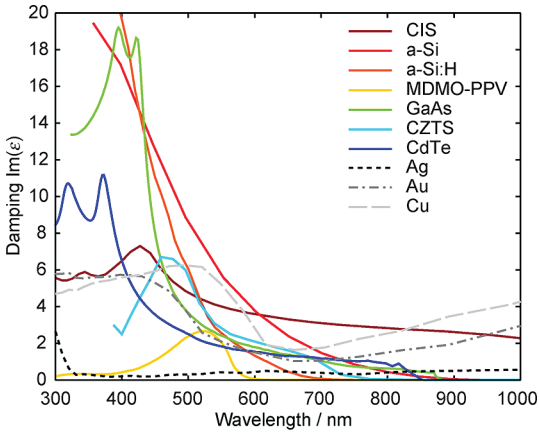

Figure 4. The damping part of the bulk permittivity is essential for the local distribution of the absorption rate in nanocomposite materials. For plasmonic solar cells it is desirable to have a low damping by the plasmonic metal (Ag, Au, and Cu shown with optical constants from ref 52) and a high damping by the thin film solar cell material [$CuInSe_2$ (CIS),[53] a-Si,[54] intrinsic a-Si:H,[55] MDMO-PPV,[56] GaAs,[54] kesterite Cu_2ZnSnS_4 (CZTS),[57] and CdTe[54] shown here].

dx.doi.org/10.1021/jz300290d | J. Phys. Chem. Lett. 2012, 3, 1275−1285

Regarding the choice of metal, the onset of interband transitions produces high damping in Cu below roughly 600 nm and in Au below about 500 nm wavelength. This makes Ag the preferred metal with respect to low losses in the visible/near-infrared. Many of the semiconductors display damping exceeding that of Ag for wavelengths slightly below their bandgap thresholds. Judged by the bulk optical constants of high damping semiconductors such as those combined with Ag, the branching ratio for semiconductor absorption can exceed 90%.[4,28] However, when the particle sizes fall below the inelastic mean free path of the metal conduction electrons, additional damping due to surface scattering also needs to be taken into account, which presumably lowers the branching ratio, as further discussed below.

When comparing different geometries, variations in the strength of coupling between the metal and semiconductor constituents affect the amount of semiconductor material needed to achieve a certain branching ratio for semiconductor absorption. From a comparison between plasmonic core/shell arrays (Figure 2a) and plasmonic arrays on top of planar semiconductor layers (Figure 2c),[15] it can be seen that for very high damping semiconductors, such that maximum absorption is realized for a small total semiconductor volume (~1 nm mass equivalent thickness), the optimal amounts of semiconductor material are very similar for these different arrangements. However, in situations of more practical interest (~10 nm mass equivalent semiconductor thickness in the core/shell array), the core/shell geometry displays the expected advantage of a more efficient coupling and gets by with 2−3 times less semiconductor material than in the "on-top" configuration. The case with a semiconductor-coated metal particle array (Figure 2d) investigated in some experimental works[17,24] is expected to perform intermediately between the on-top and core/shell ones, while the case with plasmonic particles embedded in a thin semiconductor layer (Figure 2e) is presumably very close to the core/shell situation in terms of coupling.

For applications to solar cells, it is desirable to optimize the optical properties of the device with respect to broadband absorption of sunlight. Even in the simple configurations considered here, there are typically five geometrical parameters that need to be determined by evaluation of the full spectral response. This makes analytical estimates for the absorption and how it distributes in the materials very labor-saving and useful. An optimization scheme using the integrated plasmon-induced absorption as a figure of merit[15,17] was detailed elsewhere.[28] In the end, geometries optimized by approximate analytical expressions need to be more carefully evaluated using a numerical method such as FEM. Under the assumption that all photons absorbed in the metal particles and reflector are lost as heat, and that only photons absorbed in the semiconductor contribute to the short circuit current, ideal conversion efficiencies can be estimated by multiplying the ideal Shockley−Queisser efficiencies for the bandgaps in question by the air mass 1.5G (AM1.5G)[58] weighted average of the semiconductor absorptance up to the bandgap threshold. Assuming the usage of an Al reflector, ideal conversion efficiencies in absorber arrays of Ag/CIS, Ag/a-Si, and Ag/MDMO-PPV were in this way estimated to 20, 18 and 12%, by use of 8.7, 15, and 2.3 nm mass equivalent semiconductor layer thicknesses, respectively.[28]

To refine this analysis, one should consider the contribution from surface scattering to the plasmon damping. As it turns out, the effective inelastic mean free path of the conduction electrons[59] in the optimized Ag particle cores fall below the bulk value for Ag of 51 nm. This means that electron collisions with the metal particle surfaces will significantly increase the damping of the plasmon resonance. This is likely to occur such that it contributes mainly to Joule heating of the metal, and the branching ratio for semiconductor absorption is reduced. An uncertainty here is to what extent chemical interface effects[60] involving temporary charge transfers to affinity levels close to the Fermi level at the metal/semiconductor interface, causing dephasing of the coherent resonance, will contribute, especially in the event that the semiconductor makes direct contact with the metal. An electromagnetic description based on particle bulk properties will not accurately represent the situation close to the surfaces of the metal particles. The aggregated microscopic effect on the semiconductor absorption, in particular the plasmon peak width, thus requires more detailed considerations.[61] Even though the surface effects are here assumed negative, they may under some circumstances also be favorable for solar cell applications.[62]

When applying the standard correction for surface scattering (see Computational Methods) with the effective mean free path of electrons given by a particle volume-to-surface ratio,[59] the optimal particle sizes prove larger, more spherical, and less densely packed. This turns out to challenge an analysis based on eq 1, since the point dipole approximation for the particles becomes less accurate with increased size. Grating resonances[63] further become apparent in full numerical calculations whenever the lattice constant exceeds the wavelength in the surrounding medium (that is, when $\Lambda > \lambda/n_e$). Nevertheless, if limiting the lattice constant to be less than the shortest wavelength of importance, the corresponding analytical optimum provides a useful starting point for a numerical treatment. Such an investigation shows that much of the detrimental effect of surface scattering can be counterbalanced, provided that the volume fraction of the semiconductor material in the array is increased (Figure 5a). When increasing the semiconductor shell thickness from 7.5 to 30 nm (corresponding to an increase from 3.5 to 25 nm mass equivalent thickness of semiconductor), the AM1.5G weighted average of the absorption in the wavelength range from 300 to 1192 nm (the latter being the bandgap threshold for CIS) increases from 45 to 75%. This is a combined effect of a higher branching ratio at the plasmon peak and a broader peak width. In general, overdamping the plasmonic absorber by means of a slight excess of semiconductor material is a useful strategy that allows for increasing the peak semiconductor absorption beyond that at critical coupling. The gain from overdamping is significant, especially when losses due to Joule heating of the metal is high. Because the resonance peak width is also proportional to the overall damping,[60] the benefit for the spectrally integrated absorption is twofold. Moreover, a high damping generally broadens the resonance peak as a function of geometrical parameters and thus increases the error tolerances in the system.[4] However, if the semiconductor amount is increased too much, the semiconductor peak absorption may even start to decrease at a certain point (that is, if the plasmon resonance contributes sufficiently to enhance the absorption).[15] This was recently observed experimentally.[17]

To compete efficiently with the Joule heating of the metal, especially when enhanced by surface scattering, the geometry must realize an efficient near-field coupling between the plasmon and the useful generation of electron−hole pairs in the semiconductor. On the other hand, it may be desirable to

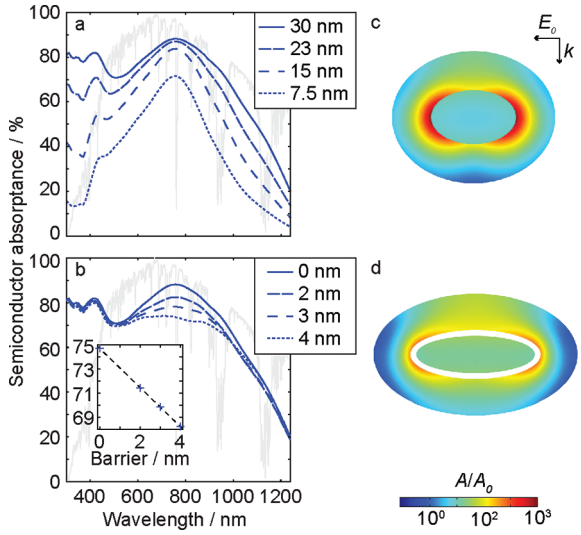

Figure 5. (a) The effect of CIS semiconductor shell thickness (7.5, 15, 23, and 30 nm, respectively) on the CIS absorption, assuming a fixed volume Ag core and taking losses due to surface scattering and an assumed Al reflector into account. The particle shapes are adjusted to compensate for shifts in the minimum reflectance (~peak absorptance) position for the different thicknesses. Grating effects manifest as sharp spectral features below about 340 nm wavelength (grating constant 170 nm, $n_e = 2$). In panel b, the effect of a dielectric barrier layer (refractive index of 2) is investigated for barrier thicknesses of 0, 2, 3, and 4 nm using the core/shell case with a 30 nm thick shell as the starting point. The metal and semiconductor volumes are maintained constant, while the particle eccentricities are again adjusted to maintain the reflectance dip position fixed when barriers of different thicknesses are introduced. The average absorptance weighted by the AM1.5G spectrum up to the bandgap threshold (at 1192 nm) decreases linearly (fitted line) with the barrier thickness, as shown in the inset. In panels c and d, the local absorption rates (A/A_0, with A_0 being a constant) are shown for cross sections of the particles having a 0 and 4 nm barrier layer, respectively. The geometries are detailed in the Supporting Information.

physically separate the semiconductor from the metal in order to avoid electron–hole pair recombination via the metal (surface) states. By using a thin, selectively electron-transmitting/hole-blocking layer or a hole-transmitting/electron-blocking layer for this purpose, efficient charge separation can be promoted,[64] but at a cost of weaker electromagnetic coupling. To shed some light on this dilemma, one should consider what happens with the semiconductor absorption if such a barrier layer is introduced. It appears feasible to accomplish barrier functions in nanometer-thick layers deposited by, for instance, atomic layer disposition (ALD)[65,66] or solution-based processing.[67,68] Thus varying the barrier thickness from 0 to 4 nm, the effect on the semiconductor absorption is seen in Figure 5b. After adjusting the particle shape to maintain the peak position and the volume of absorbing material, it is found that the main effect of a barrier layer is to "shave off" the absorption peak, with absorption on the sides of the peak remaining relatively intact. The AM1.5G spectrally weighted absorptance decreases moderately, and, to good approximation, linearly with the barrier thickness, from 75 to 68% when going from 0 to 4 nm barriers in these examples (inset of Figure 5b). Distributions of local absorption rates are shown for the two extreme cases in Figure 5c,d. Thus, when the particles are fairly large compared to the thickness of the barrier, the near-field can extend sufficiently beyond it, and the loss in coupling strength does not dramatically alter the absorption distribution. On the basis of an ideal efficiency of 31.2%[69] for the CIS bandgap of 1.04 eV,[53] an average of around 70% absorption corresponds to a 22% ideal conversion efficiency.

Since the highest thin film efficiencies presently achieved are approximately 20% (for CIGS[70]), it can thus be concluded that even when taking surface scattering, barrier layers to prevent surface recombination, and nonideal reflectors into account, plasmonic near-field absorbers have the optical capacity to match the record efficiencies presently achieved in comparable thin film solar cells while using only one hundredth of the amount of absorber material. The possible efficiency range is of course dependent on which figure of merit is chosen for the optimization. Without any other constraints imposed on a theoretical maximization of the efficiency, it would reproduce the ideal Shockley–Queisser limit for an optically thick film of the semiconductor bandgap in question. However, if the levelized cost of electricity is the final target rather than the efficiency, a more interesting question is perhaps how high of a conversion efficiency can be obtained for a given amount of absorber material. For ultrathin systems, plasmonic near-field absorbers stand out at as one of the most promising candidates in this respect. An ideal efficiency comparison based on the examples presented in Figure 5 and the fully optimized (that is, with respect to the AM1.5G integrated absorption) planar configurations of a CIS film/spacer/Al reflector is provided in Figure 6. Note that the angular spread of sunlight and the

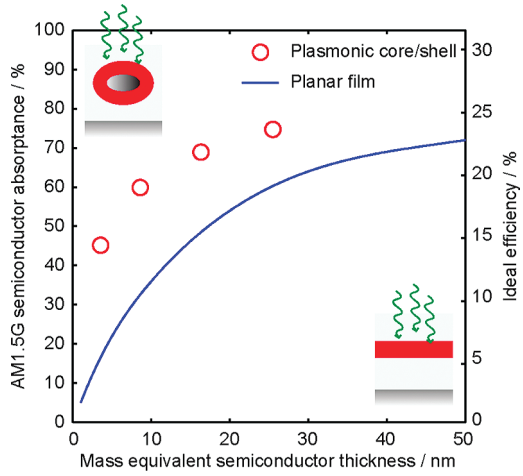

Figure 6. Average semiconductor absorptance and the corresponding ideal efficiency as a function of the amount of semiconductor material. The integrated semiconductor absorptance based on the spectra of Figure 5a for Ag core/CIS shell arrays (upper left cartoon) is compared to that of fully optimized stacks with a planar CIS film alone (lower right cartoon). A dielectric environment ($n_i = n_s = 2$) and an Al back reflector are considered in both cases. Normal incidence of AM1.5G light is assumed. The geometries are detailed in the Supporting Information.

dependence on film thickness for the open circuit voltage were not accounted for, and that these effects would be in favor of small thicknesses.

The efficiency numbers cited here for Ag core/CIS shell arrays are found by using the integrated plasmon-induced absorptance. That is, the vertical gap between the curve for the planar and the core/shell efficiencies of Figure 6 is used as guidance. However, these examples should not be considered fully optimized, as the analytical model used for a starting point

dx.doi.org/10.1021/jz300290d | J. Phys. Chem. Lett. 2012, 3, 1275–1285

is not able to account well for the absorption in the blue range where the particle size is appreciable compared to the wavelength. In fact, an optimum found using the analytical approximation of eq 1 tends to be underdamped, so that critical coupling is reached in a full FEM calculation only after addition of more semiconductor material (Figure 5a) or by spacing the particles further apart. Thus, although all relevant parameters of the system were included in the present analysis, a more detailed analytical approximation for the effective optical properties of the absorber layer, taking higher orders of poles and array interactions into account, could with high likelihood be used to identify still better conditions.

It can thus be concluded that even when taking surface scattering, barrier layers to prevent surface recombination, and nonideal reflectors into account, plasmonic near-field absorbers have the optical capacity to match the record efficiencies presently achieved in comparable thin film solar cells while using only one hundredth of the amount of absorber material.

Apart from a further refined theoretical analysis of the optimal conditions in ordered arrays, many interesting questions and challenges remain to be addressed relating to solar cells based on these plasmonic near-field absorbers. Further elucidation is desirable with regards to the role of large scale order in the system, especially in relation to branching ratios (disordered systems are often easier to fabricate, while ordered systems are more readily analyzed and optimized). The effect of chemical interface damping needs further investigation, especially in situations where the semiconductor is in direct contact with the metal. Further, the optical response has only recently been coupled to the charge transport in models.[71] On the experimental side, it is challenging to really optimize all parameters with respect to near-field absorption, and, for instance, the semiconductor layer thickness is an often overlooked parameter.[17] Some systems investigated do come close to those geometries considered here, for instance with a-Si:H[17,24] and organic solar cell layers.[72] However, much work remains not only to fabricate optically high performing structures, but to integrate them in device configurations allowing for efficient charge carrier extraction and electronic output. This requires the use of transparent materials able to form appropriate contacts with the absorber layer and transport charge carriers, without causing significant losses in the form of free carrier absorption.

Looking forward, the concept of combining a near-zero effective thickness plasmonic near-field absorber with an effectively zero path length reflector cavity can readily be extended to increase the absorption bandwidth further. Since optical analogues of electric and, to some extent, magnetic layers ("screens") can be accomplished using these ultrathin plasmonic nanocomposites, one may find inspiration in technology building further on the Salisbury screen.[35] The use of resonances with magnetic components is attractive due to the very broad spectral features demonstrated and potentially simple implementation (Figure 7a), but it remains to be seen if

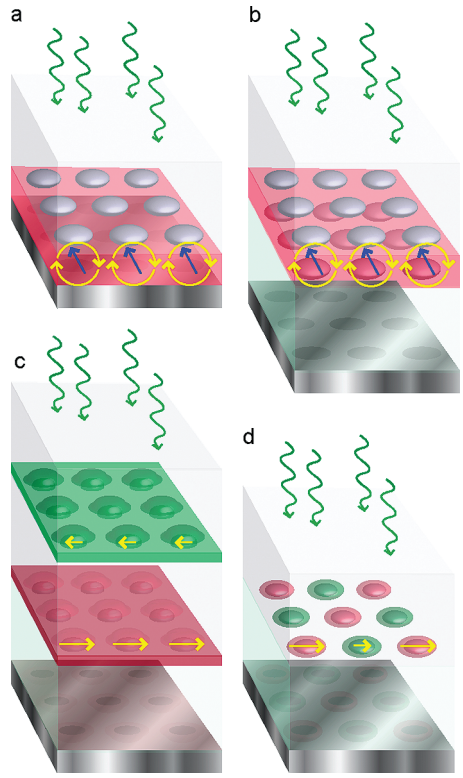

Figure 7. Alternative configurations of potential interest for broadening the absorption in ultrathin semiconductor layers based on plasmonic near-field effects and a back reflector. Characteristic electric (yellow) and magnetic (blue) field lines for the targeted resonance modes are indicated. (a) A metal nanoparticle array characterized by a magnetic metamaterial response, which induces absorption in a thin semiconductor film inserted between the array and reflector. (b) A magnetic metamaterial absorber in a more freely tunable configuration with a back reflector. (c) A tandem absorber layer/spacer layer configuration taking advantage of electric resonances. (d) Two interspersed core/shell arrays having the potential to produce critical coupling at more than one wavelength.

this is compatible with a significant fraction of the light absorption being channeled to a semiconductor material, presumably located between the array and a back reflector where the field of this resonance is focused. As the optimal distance for near-field coupling between the array and the reflector to create a strong magnetic response is unlikely to coincide with the optimal thickness (damping) of the semiconductor, one may consider the introduction of additional degrees of freedom in the form of, for instance, another array of particles and a spacer layer (Figure 7b). Another intriguing prospect is to combine several layers into a mainly electric mode stack (Figure 7c). Even in tandem configurations with only two layers, the stack allows for a "maximally flat" optical response to be realized.[35] This implies a broader spectral coverage of the absorption. In combination with a bandgap optimization along the lines of conventional tandem solar cells, very high efficiencies could be expected with extremely small amounts of light-absorbing material.

dx.doi.org/10.1021/jz300290d | J. Phys. Chem. Lett. 2012, 3, 1275−1285

The concept of combining a near-zero effective thickness plasmonic near-field absorber with an effectively zero path length reflector cavity can readily be extended to increase the absorption bandwidth further.

A somewhat related approach to increase the absorption peak width is to use interspersed two-dimensional lattices of two or more nanoparticle types (core/shell or similar), providing oscillator strength in different parts of the spectrum such that critical coupling can be achieved at two or more wavelengths (Figure 7d). If such arrays could be fabricated, even simple core/shell spheroids should provide sufficient degrees of freedom (that is, at least two to match the optimal n_{eff} and k_{eff}) to tune the system to one critical coupling wavelength per particle type. More generally, the use of particle size, shape, or distribution heterogeneities is a feasible approach to broaden the absorption spectrum,[73] but it is less clear how well this type of broadening will translate to the production of useful charge carriers via the near-field.[17]

The concepts discussed in this Perspective apply to a broad range of thin film solar cell materials such as those exemplified in Figure 4, and are also of high relevance for photochemical energy conversion, as recently shown in several works.[74−77] The basic requirements for the semiconductor materials are that they are sufficiently absorbing (damping) to compete well with Joule heating of the metallic elements and that they can be grown in a controlled and preferably uniform fashion with typical thicknesses around 10 nm.

To summarize, the versatility of ultrathin plasmonic nanocomposites allows for their optical properties to be adjusted to nearly ideal conditions for solar energy conversion, in the sense that high absorption can be achieved over a wide part of the solar spectrum. By exploiting the enhanced near-fields around the plasmonic constituents, a large fraction of the absorbed power can be channeled to a semiconductor material where electron−hole pairs feasible for charge carrier extraction are produced. This near-field mechanism is particularly powerful in strongly coupled systems of optically low damping metals such as silver and high damping semiconductors common in thin films solar cells. Geometries realizing a strong electromagnetic coupling between the metal, where the plasmon resonance is centered, and the semiconductor material, where absorption is desirable, are those where the semiconductor is in direct contact with the metal and bounded outward by an isosurface of electric field energy (absorption rate). Metal core/semiconductor shell nanoparticles come close to this ideal, but some other structures (semiconductor coated or embedded arrays of metal nanoparticles) do not show strong disadvantages in this respect. It is also possible to include thin (~nanometer) passivating layers between the metal and semiconductor constituents without causing more than moderate losses in semiconductor absorption; the spectrally integrated loss of absorption is found to be directly proportional to the barrier thickness and can be made small by increasing the amount of semiconductor material. As an example, a 68% average absorptance in a $CuInSe_2$ semiconductor having a mass equivalent thicknesses of 25 nm was achieved with a 4-nm-thick dielectric barrier between the metal and semiconductor. This implies an ideal solar energy conversion efficiency around 21% with losses due to surface scattering and a nonideal Al back reflector taken into account. The advantage of plasmonic absorbers over fully optimized planar configurations of conventional absorber layers is clarified further by displaying calculated efficiencies as a function of the amount of semiconductor material used.

The behavior of ultrathin plasmonic near-field absorbers as essentially zero thickness layers allows for envisioning more advanced stacks of such layers enabling broader spectral responses, which improve on the demonstrated capability of the Salisbury screen configuration. If this can be combined with reduced electron−hole pair thermalization losses in the semiconductors through appropriate bandgap matching of the different layers, the higher ideal efficiencies of multijunction solar cells can be approached with extremely small amounts of material. The use of magnetic type resonances is another exciting direction to look further into. Thus the advancement of ultrathin plasmonic near-field absorbers is anticipated to be a fruitful area of research in combination with refined techniques for controlled assembly of plasmonic nanostructures and conformal growth of semiconductor materials on the nanoscale, such as by atomic layer deposition and solution-based methods.

■ COMPUTATIONAL METHODS

Calculations by the FEM were performed using software from COMSOL Multiphysics as described in more detail elsewhere.[28,78] Correction for surface scattering for the Ag particle permittivity was implemented according to eq 1.4 of ref 59 with the prefactor A taken to unity and the effective inelastic mean free path $l_{eff} = 4V/S$, with S being the metal particle surface area and V its volume. The properties of Ag were further represented by a bulk inelastic mean free path of 51 nm based on its direct current (dc) conductivity, a bulk plasmon resonance energy of 9.2 eV, and a Fermi velocity of 1.39×10^6 m/s. The Al reflector was implemented as an impedance boundary condition using tabulated optical constants.[79]

■ ASSOCIATED CONTENT

Supporting Information

Geometrical parameters for the calculations presented in Figures 5 and 6. This material is available free of charge via the Internet at http://pubs.acs.org.

■ AUTHOR INFORMATION

Corresponding Author

*E-mail: hagglund@stanford.edu.

Notes

The authors declare no competing financial interest.

Biographies

Carl Hägglund received his Ph.D. from the Department of Applied Physics at Chalmers University of Technology, Sweden, with a focus on the plasmonic enhancement of photocurrents in dye-sensitized and silicon solar cells and the optimization of plasmonic solar cells. He is currently a postdoctoral researcher at the Department of Chemical Engineering, Stanford University, USA, continuing work on plasmonic photovoltaics with atomic layer deposition as a new ingredient.

S. Peter Apell is a professor of Physics at the Department of Applied Physics at Chalmers University of Technology, Sweden. He has worked on plasmons on and off for the last 30 years addressing various

topics ranging from basic questions connected to electron spill-out to applications for sensing and energy harvesting. His main research interests are currently with graphene plasmonics.

■ ACKNOWLEDGMENTS

The authors thank Viktoria Gusak and Jim Robinson for valuable comments on the manuscript. C.H. performed this work within the Center on Nanostructuring for Efficient Energy Conversion (CNEEC) at Stanford and is grateful for funding from the Marcus and Amalia Wallenberg Foundation. S.P.A. acknowledges support from the Swedish Foundation for Strategic Research via the Functional Electromagnetic Metamaterials project SSF RMA08.

■ REFERENCES

(1) Sanden, B. Solar Solution: The Next Industrial Revolution. *Mater. Today* **2008**, *11*, 22−24.
(2) Atwater, H. A.; Polman, A. Plasmonics for Improved Photovoltaic Devices. *Nat. Mater.* **2010**, *9*, 205−213.
(3) Atkins, P. W.; Friedman, R. S. *Molecular Quantum Mechanics*, 4th ed.; Oxford University Press: New York, 2005.
(4) Hägglund, C.; Apell, S. P.; Kasemo, B. Maximized Optical Absorption in Ultrathin Films and Its Application to Plasmon-Based Two-Dimensional Photovoltaics. *Nano Lett.* **2010**, *10*, 3135−3141.
(5) Queisser, H. J. Photovoltaic Conversion at Reduced Dimensions. *Physica E* **2002**, *14*, 1−10.
(6) Bohren, C. F.; Huffman, D. R. *Absorption and Scattering of Light by Small Particles.*: Wiley-VCH: Weinheim, Germany, 1998; p 544.
(7) Jackson, J. D. *Classical Electrodynamics*, 3rd ed.; John Wiley & Sons, Inc.: New York, 1999.
(8) Westphalen, M.; Kreibig, U.; Rostalski, J.; Luth, H.; Meissner, D. Metal Cluster Enhanced Organic Solar Cells. *Sol. Energy Mater. Sol. Cells* **2000**, *61*, 97−105.
(9) Tian, Y.; Tatsuma, T. Mechanisms and Applications of Plasmon-Induced Charge Separation at TiO_2 Films Loaded with Gold Nanoparticles. *J. Am. Chem. Soc.* **2005**, *127*, 7632.
(10) Hertel, T.; Knoesel, E.; Wolf, M.; Ertl, G. Ultrafast Electron Dynamics at Cu(111): Response of an Electron Gas to Optical Excitation. *Phys. Rev. Lett.* **1996**, *76*, 535−538.
(11) Langhammer, C.; Kasemo, B.; Zoric, I. Absorption and Scattering of Light by Pt, Pd, Ag, and Au Nanodisks: Absolute Cross Sections and Branching Ratios. *J. Chem. Phys.* **2007**, *126*, 194702−11.
(12) Pala, R. A.; White, J.; Barnard, E.; Liu, J.; Brongersma, M. L. Design of Plasmonic Thin-Film Solar Cells with Broadband Absorption Enhancements. *Adv. Mater.* **2009**, *21*, 3504.
(13) Lee, J.-Y.; Peumans, P. The Origin of Enhanced Optical Absorption in Solar Cells with Metal Nanoparticles Embedded in the Active Layer. *Opt. Express* **2010**, *18*, 10078−10087.
(14) Mendes, M. J.; Luque, A.; Tobias, I.; Marti, A. Plasmonic Light Enhancement in the Near-Field of Metallic Nanospheroids for Application in Intermediate Band Solar Cells. *Appl. Phys. Lett.* **2009**, *95*, 071105−3.
(15) Hägglund, C.; Kasemo, B. Nanoparticle Plasmonics for 2D-Photovoltaics: Mechanisms, Optimization, and Limits. *Opt. Express* **2009**, *17*, 11944−11957.
(16) García de Arquer, F. P.; Beck, F. J.; Konstantatos, G. Absorption Enhancement in Solution Processed Metal-Semiconductor Nanocomposites. *Opt. Express* **2011**, *19*, 21038−21049.
(17) Gusak, V.; Kasemo, B.; Hägglund, C. Thickness Dependence of Plasmonic Charge Carrier Generation in Ultrathin a-Si:H Layers for Solar Cells. *ACS Nano* **2011**, *5*, 6218−6225.
(18) Hägglund, C.; Zäch, M.; Kasemo, B. Enhanced Charge Carrier Generation in Dye Sensitized Solar Cells by Nanoparticle Plasmons. *Appl. Phys. Lett.* **2008**, *92*, 013113.
(19) Stuart, H. R.; Hall, D. G. Absorption Enhancement in Silicon-on-Insulator Waveguides Using Metal Island Films. *Appl. Phys. Lett.* **1996**, *69*, 2327−2329.
(20) Mallick, S. B.; Sergeant, N. P.; Agrawal, M.; Lee, J.-Y.; Peumans, P. Coherent Light Trapping in Thin-Film Photovoltaics. *MRS Bull.* **2011**, *36*, 453−460.
(21) Beck, F. J.; Polman, A.; Catchpole, K. R. Tunable Light Trapping for Solar Cells Using Localized Surface Plasmons. *J. Appl. Phys.* **2009**, *105*.
(22) Wang, F.; Shen, Y. R. General Properties of Local Plasmons in Metal Nanostructures. *Phys. Rev. Lett.* **2006**, *97*, 206806.
(23) Bakke, J. R.; Pickrahn, K. L.; Brennan, T. P.; Bent, S. F. Nanoengineering and Interfacial Engineering of Photovoltaics by Atomic Layer Deposition. *Nanoscale* **2011**, *3*, 3482−3508.
(24) Moulin, E.; Luo, P. Q.; Pieters, B.; Sukmanowski, J.; Kirchhoff, J.; Reetz, W.; Muller, T.; Carius, R.; Royer, F. X.; Stiebig, H. Photoresponse Enhancement in the near Infrared Wavelength Range of Ultrathin Amorphous Silicon Photosensitive Devices by Integration of Silver Nanoparticles. *Appl. Phys. Lett.* **2009**, *95*, 033505.
(25) Rand, B. P.; Peumans, P.; Forrest, S. R. Long-Range Absorption Enhancement in Organic Tandem Thin-Film Solar Cells Containing Silver Nanoclusters. *J. Appl. Phys.* **2004**, *96*, 7519−7526.
(26) Bedeaux, D.; Vlieger, J. *Optical Properties of Surfaces*, 2nd ed.; Imperial College Press: London, 2004; p 450.
(27) Vlieger, J. Reflection and Transmission of Light by a Square Nonpolar Lattice. *Physica* **1973**, *64*, 63−81.
(28) Hägglund, C.; Apell, S. P. Resource Efficient Plasmon-Based 2D-Photovoltaics with Reflective Support. *Opt. Express* **2010**, *18*, A343−A356.
(29) Vernon, K. C.; Funston, A. M.; Novo, C.; Gómez, D. E.; Mulvaney, P.; Davis, T. J. Influence of Particle−Substrate Interaction on Localized Plasmon Resonances. *Nano Lett.* **2010**, *10*, 2080−2086.
(30) Di Biasio, A.; Ambrosone, L.; Cametti, C. Dielectric Properties of Biological Cells in the Dipolar Approximation for the Single-Shell Ellipsoidal Model: The Effect of Localized Surface Charge Distributions at the Membrane Interface. *Phys. Rev. E* **2010**, *82*, 041916.
(31) Hägglund, C.; Apell, S. P.; Kasemo, B. Maximized Optical Absorption in Ultrathin Films and Its Application to Plasmon-Based Two-Dimensional Photovoltaics [*Nano Lett.*, 2010, *10*, 3135]. *Nano Lett.* **2011**, *11*, 915−916.
(32) Mendoza-Galván, A.; Järrendahl, K.; Dmitriev, A.; Pakizeh, T.; Käll, M.; Arwin, H. Optical Response of Supported Gold Nanodisks. *Opt. Express* **2011**, *19*, 12093−12107.
(33) Alu, A.; Silveirinha, M. G.; Salandrino, A.; Engheta, N. Epsilon-Near-Zero Metamaterials and Electromagnetic Sources: Tailoring the Radiation Phase Pattern. *Phys. Rev. B* **2007**,*75*.
(34) Salisbury, W. W. Absorbent Body for Electromagnetic Waves. U.S. Patent 2599944, June 10, 1952.
(35) Fante, R. L.; McCormack, M. T. Reflection Properties of the Salisbury Screen. *IEEE Trans. Antennas Propag.* **1988**, *36*, 1443−1454.
(36) Tischler, J. R.; Bradley, M. S.; Bulovic, V. Critically Coupled Resonators in Vertical Geometry Using a Planar Mirror and a 5 nm Thick Absorbing Film. *Opt. Lett.* **2006**, *31*, 2045−2047.
(37) Gupta, S. D. Strong-Interaction-Mediated Critical Coupling at Two Distinct Frequencies. *Opt. Lett.* **2007**, *32*, 1483−1485.
(38) Driessen, E. F. C.; de Dood, M. J. A. The Perfect Absorber. *Appl. Phys. Lett.* **2009**, *94*, 171109.
(39) Laroche, M.; Albaladejo, S.; Gomez-Medina, R.; Saenz, J. J. Tuning the Optical Response of Nanocylinder Arrays: An Analytical Study. *Phys. Rev. B* **2006**, *74*, 245422.
(40) de Abajo, F. J. G. Colloquium: Light Scattering by Particle and Hole Arrays. *Rev. Mod. Phys.* **2007**, *79*, 1267−1290.
(41) Thongrattanasiri, S.; Koppens, F. H. L.; García de Abajo, F. J. Complete Optical Absorption in Periodically Patterned Graphene. *Phys. Rev. Lett.* **2012**, *108*, 047401.
(42) Hedayati, M. K.; Javaherirahim, M.; Mozooni, B.; Abdelaziz, R.; Tavassolizadeh, A.; Chakravadhanula, V. S. K.; Zaporojtchenko, V.; Strunkus, T.; Faupel, F.; Elbahri, M. Design of a Perfect Black

Absorber at Visible Frequencies Using Plasmonic Metamaterials. *Adv. Mater.* **2011**, *23*, 5410−5414.
(43) Landy, N. I.; Sajuyigbe, S.; Mock, J. J.; Smith, D. R.; Padilla, W. J. Perfect Metamaterial Absorber. *Phys. Rev. Lett.* **2008**, 100.
(44) Diem, M.; Koschny, T.; Soukoulis, C. M. Wide-Angle Perfect Absorber/Thermal Emitter in the Terahertz Regime. *Phys. Rev. B* **2009**,*79*.
(45) Hao, J.; Wang, J.; Liu, X.; Padilla, W. J.; Zhou, L.; Qiu, M. High Performance Optical Absorber Based on a Plasmonic Metamaterial. *Appl. Phys. Lett.* **2010**, *96*, 251104−3.
(46) Liu, N.; Mesch, M.; Weiss, T.; Hentschel, M.; Giessen, H. Infrared Perfect Absorber and Its Application as Plasmonic Sensor. *Nano Lett.* **2010**, *10*, 2342−2348.
(47) Chen, H.-T. Interference Theory of Metamaterial Perfect Absorbers. http://arxiv.org/abs/1112.5168, 2011.
(48) Hao, J.; Zhou, L.; Qiu, M. Nearly Total Absorption of Light and Heat Generation by Plasmonic Metamaterials. *Phys. Rev. B* **2011**, *83*, 165107.
(49) Zeng, Y.; Chen, H.-T.; Dalvit, D. A. R. A Reinterpretation of the Metamaterial Perfect Absorber.http://arxiv.org/abs/1201.5109, 2012.
(50) Seah, M. P.; Dench, W. A. Quantitative Electron Spectroscopy of Surfaces: A Standard Data Base for Electron Inelastic Mean Free Paths in Solids. *Surf. Interface Anal.* **1979**, *1*, 2−11.
(51) Knight, M. W.; Sobhani, H.; Nordlander, P.; Halas, N. J. Photodetection with Active Optical Antennas. *Science* **2011**, *332*, 702−704.
(52) Johnson, P. B.; Christy, R. W. Optical-Constants of Noble-Metals. *Phys. Rev. B* **1972**, *6*, 4370−4379.
(53) Alonso, M. I.; Wakita, K.; Pascual, J.; Garriga, M.; Yamamoto, N. Optical Functions and Electronic Structure of $CuInSe_2$, $CuGaSe_2$, $CuInS_2$, and $CuGaS_2$. *Phys. Rev. B* **2001**, *63*, 075203.
(54) Palik, E. D. *Handbook of Optical Constants of Solids*; Elsevier: New York, 1998.
(55) Schropp, R. E. I.; Zeman, M. *Amorphous and Microcrystalline Silicon Solar Cells: Modeling, Materials and Device Technology*; Kluwer Academic Publishers: Boston/Dordrecht/London, 1998; p 207.
(56) Hoppe, H.; Sariciftci, N. S.; Meissner, D. Optical Constants of Conjugated Polymer/Fullerene Based Bulk-Heterojunction Organic Solar Cells. *Mol. Cryst. Liq. Cryst.* **2002**, *385*, 233−239.
(57) Persson, C. Electronic and Optical Properties of Cu_2ZnSnS_4 and $Cu_2ZnSnSe_4$. *J. Appl. Phys.* **2010**, *107*, 053710.
(58) NREL Reference Solar Spectral Irradiance: Air Mass 1.5. http://rredc.nrel.gov/solar/spectra/am1.5/.
(59) Coronado, E. A.; Schatz, G. C. Surface Plasmon Broadening for Arbitrary Shape Nanoparticles: A Geometrical Probability Approach. *J. Chem. Phys.* **2003**, *119*, 3926−3934.
(60) Hövel, H.; Fritz, S.; Hilger, A.; Kreibig, U.; Vollmer, M. Width of Cluster Plasmon Resonances: Bulk Dielectric Functions and Chemical Interface Damping. *Phys. Rev. B* **1993**, *48*, 18178−18188.
(61) Pinchuk, A. O.; Kreibig, U. Interface Decay Channel of Particle Surface Plasmon Resonance. *New J. Phys.* **2003**, *5*, 151.
(62) Larkin, I. A.; Stockman, M. I.; Achermann, M.; Klimov, V. I. Dipolar Emitters at Nanoscale Proximity of Metal Surfaces: Giant Enhancement of Relaxation in Microscopic Theory. *Phys. Rev. B* **2004**, *69*, 121403(R).
(63) Lamprecht, B.; Schider, G.; Lechner, R. T.; Ditlbacher, H.; Krenn, J. R.; Leitner, A.; Aussenegg, F. R. Metal Nanoparticle Gratings: Influence of Dipolar Particle Interaction on the Plasmon Resonance. *Phys. Rev. Lett.* **2000**, *84*, 4721−4724.
(64) Fonash, S. J. *Solar Cell Device Physics*, 2nd ed.; Academic Press: Burlington, MA, 2010; p 353.
(65) Standridge, S. D.; Schatz, G. C.; Hupp, J. T. Toward Plasmonic Solar Cells: Protection of Silver Nanoparticles via Atomic Layer Deposition of TiO_2. *Langmuir* **2009**, *25*, 2596−2600.
(66) Tien, T.-C.; Pan, F.-M.; Wang, L.-P.; Tsai, F.-Y.; Lin, C. Coverage Analysis for the Core/Shell Electrode of Dye-Sensitized Solar Cells. *J. Phys. Chem. C* **2010**, *114*, 10048−10053.
(67) Fan, S.-Q.; Geng, Y.; Kim, C.; Paik, S.; Ko, J. Correlating the Photovoltaic Performance of Alumina Modified Dye-Sensitized Solar Cells with the Properties of Metal-Free Organic Sensitizers. *Mater. Chem. Phys.* **2012**, *132*, 943−949.
(68) Qi, J.; Dang, X.; Hammond, P. T.; Belcher, A. M. Highly Efficient Plasmon-Enhanced Dye-Sensitized Solar Cells through Metal@Oxide Core−Shell Nanostructure. *ACS Nano* **2011**, *5*, 7108−7116.
(69) Bolton, J. R.; Archer, M. D. Requirements for Ideal Performance of Photochemical and Photovoltaic Solar Energy Converters. *J. Phys. Chem.* **1990**, *94*, 8028−8036.
(70) Green, M. A.; Emery, K.; Hishikawa, Y.; Warta, W. Solar Cell Efficiency Tables (Version 34). *Prog. Photovoltaics* **2009**, *17*, 320−326.
(71) Li, X.; Hylton, N. P.; Giannini, V.; Lee, K.-H.; Ekins-Daukes, N. J.; Maier, S. A. Bridging Electromagnetic and Carrier Transport Calculations for Three-Dimensional Modelling of Plasmonic Solar Cells. *Opt. Express* **2011**, *19*, A888−A896.
(72) Kulkarni, A. P.; Noone, K. M.; Munechika, K.; Guyer, S. R.; Ginger, D. S. Plasmon-Enhanced Charge Carrier Generation in Organic Photovoltaic Films Using Silver Nanoprisms. *Nano Lett.* **2010**, *10*, 1501−1505.
(73) Aydin, K.; Ferry, V. E.; Briggs, R. M.; Atwater, H. A. Broadband Polarization-Independent Resonant Light Absorption Using Ultrathin Plasmonic Super Absorbers. *Nat. Commun.* **2011**, *2*, 517.
(74) Thomann, I.; Pinaud, B. A.; Chen, Z.; Clemens, B.; Jaramillo, T. F.; Brongersma, M. L. Plasmon Enhanced Solar-to-Fuel Energy Conversion. *Nano Lett.* **2011**, *11*, 3440−3446.
(75) Warren, S. C.; Thimsen, E. Plasmonic Solar Water Splitting. *Energy Environ. Sci.* **2012**, *5*, 5133−5146.
(76) Zhdanov, V. P.; Kasemo, B. Photo-Induced Chemical Processes on Metal−Semiconductor−Metal Nanostructures. *Chem. Phys. Lett.* **2012**, *524*, 16−19.
(77) Gao, H.; Liu, C.; Jeong, H. E.; Yang, P. Plasmon-Enhanced Photocatalytic Activity of Iron Oxide on Gold Nanopillars. *ACS Nano* **2011**, *6*, 234−240.
(78) Hägglund, C.; Zäch, M.; Petersson, G.; Kasemo, B. Electromagnetic Coupling of Light into a Silicon Solar Cell by Nanodisk Plasmons. *Appl. Phys. Lett.* **2008**, *92*, 053110.
(79) Weaver, J. H.; Frederikse, H. P. R. Optical Properties of Selected Elements. In *CRC Handbook of Chemistry and Physics*, 83 ed.; Lide, D. R., Ed. CRC Press: Boca Raton, FL, 2002.